Seismicity at the southern East Pacific Rise from recordings of an ocean bottom seismometer array

Yang Shen

University of Rhode Island, Graduate School of Oceanography, Narragansett, Rhode Island, USA

Received 29 December 2001; revised 1 May 2002; accepted 9 May 2002; published 26 December 2002.

[1] Seismic data recorded by ocean bottom seismometers (OBSs) at the southern East Pacific Rise (SEPR) were analyzed to characterize seismicity at fast spreading mid-ocean ridges. An automated event detection algorithm based on pattern recognition was developed to identify earthquake-generated T phases. The waveform cross-correlation and least squares method was found to provide more robust estimates of T phase relative travel times than the method of picking T phase maximum amplitude. The OBSs and subsequent equatorial Pacific hydrophones recorded earthquakes near an earthquake swarm in 1992, which was located ~300 km west of the ridge axis at about 18°S and 116°W. The process that generated the 1992 swarm either was reactivated 3 years later during the OBS experiment or has been continuously active in the past decade. This long-term activity suggests renewable stresses, which are consistent with the interpretation that magma injection was the cause of the 1992 swarm. In contrast to the swarm characteristics of earthquakes on the west flank of the ridge axis, earthquakes on the Nazca flank were randomly distributed in time and space. This difference in seismicity may result from the difference in the thermal structure of the Pacific and Nazca plates. The few earthquakes located at or near the ridge axis had very small magnitudes, reflecting the presence of shallow magma chambers and the thin elastic layer of the SEPR. This result suggests that acoustic monitoring of earthquakes associated with dike intrusion is difficult at regional scales at the SEPR. There is no apparent correlation between seismicity and off-axis seamounts. *INDEX TERMS:* 3025 Marine Geology and Geophysics: Marine seismics (0935); 3035 Marine Geology and Geophysics: Midocean ridge processes; 4259 Oceanography: General: Ocean acoustics; 7230 Seismology: Seismicity and seismotectonics; 9355 Information Related to Geographic Region: Pacific Ocean; *KEYWORDS:* T phase, ocean bottom seismology, mid-ocean ridges, East Pacific Rise, marine seismics, seismicity

Citation: Shen, Y., Seismicity at the southern East Pacific Rise from recordings of an ocean bottom seismometer array, *J. Geophys. Res.*, *107*(B12), 2368, doi:10.1029/2001JB001742, 2002.

1. Introduction

[2] The southern East Pacific Rise (SEPR) has few earthquakes that are detectable by land-based seismic networks. Yet several geological processes at this fast spreading (145 mm/yr, full rate), mid-ocean ridge are expected to generate earthquakes, albeit at low magnitudes. The SEPR is characterized by a valley 10–200 m deep along most of the ridge axis, which may initiate as a linear version of caldera collapse [*Macdonald and Fox*, 1988; *Haymon et al.*, 1991; *Fornari et al.*, 1997] or a graben associated with dike intrusion [*Chadwick*, 1997]. With some exceptions, axial summit calderas or grabens are found to coincide with axial magma chambers (AMC) [*Macdonald and Fox*, 1988; *Detrick et al.*, 1993; *Scheirer et al.*, 1996]. As the lithosphere thickens and strengthens sufficiently to support shear failure, the caldera eventually becomes bounded by true normal faults and the axial summit caldera becomes the axial summit graben [*Carbotte and Macdonald*, 1994; *Sinton et al.*, 1991; *Auzende et al.*, 1996]. Faulting may continue to at least 30-km off-axis, as inferred from measurements of the height of fault scarps at the northern East Pacific Rise [*Lee and Solomon*, 1995; *Macdonald et al.*, 1996]. The formation and evolution of the axial summit caldera, the accumulation and redistribution of magma, and the extension of the ridge axis may all cause seismogenic failure.

[3] It is unclear whether off-axis volcanism, abundant near the SEPR [*Shen et al.*, 1993, 1995; *Scheirer et al.*, 1996], is associated with seismic activities. Also poorly known are background levels and causes of off-axis, intraplate seismicity. Several sources of stress, such as ridge push [e.g., *Okal et al.*, 1980], cooling of the lithosphere [e.g., *Bergman and Solomon*, 1984; *Wiens and Stein*, 1984; *Bratt et al.*, 1985; *Denlinger and Savage*, 1989], loading by local topographic features, and volcanic activity [*Wysession et al.*, 1991], have been proposed for various oceanic intraplate earthquakes. In this particular region, north-south extension of the Pacific plate [*Sandwell et al.*, 1995], which has been proposed to explain gravity lineations in the

0148-0227/02/2001JB001742$09.00

central Pacific [*Haxby and Weissel*, 1986], is also a possible source of tectonic stress. *Wysession et al.* [1991] cataloged 403 reliable, intraplate earthquakes in the Pacific Basin occurred during the period of 1913–1988. While many of these earthquakes were associated with known tectonic and bathymetric features such as diffuse plate boundaries, fossil spreading ridges, and seamounts, some were not associated with any obvious feature [*Wysession et al.*, 1991, 1995] and thus represented the background seismicity. Stress orientations inferred from the background seismicity were consistent with the hypothesis that they were controlled by the relief of thermoelastic stresses [*Wiens and Stein*, 1983, 1984; *Bergman and Solomon*, 1984; *Bratt et al.*, 1985]. Oceanic intraplate earthquakes recorded by land-based seismometers are few in number, however, and it is unclear whether their distribution and occurrence rate are random or a function of the seafloor subsidence rate as expected from cooling of the oceanic lithosphere. A better characterization of the distribution and rate of intraplate earthquakes requires recording of much more frequent microseismicity.

[4] Between November 1995 and May 1996, 51 ocean bottom seismometers (OBSs) were deployed on the SEPR near 17°S (Figure 1) in the Mantle Electromagnetic and Tomography (MELT) experiment [*Forsyth et al.*, 1998]. Continuous seismic data recorded by the OBS array during the 6-month period provided a rare opportunity to characterize seismicity at this fast spreading, mid-ocean ridge. This paper presents analyses of the local seismicity recorded by the MELT OBS array and its relationship to on- and off-axis tectonic and volcanic activities.

2. Experiment Setting and Seismic Data

[5] The MELT experiment was located at a segment of the spreading center that is remarkably linear from the Garrett Transform Fault to an overlapping spreading center (OSC) near 20°40′S (Figure 1). On a finer scale, the plate boundary is offset en echelon by a series of small, left-stepping discontinuities [*Lonsdale*, 1989; *Sinton et al.*, 1991; *Cormier et al.*, 1996]. This portion of the ridge is underlain by the shallowest known axial magma chamber, only about 1–1.3 km beneath the seafloor [*Detrick et al.*, 1993]. Submersible and towed camera surveys show that the areas around 17–17°30′S and 18°35′S have recent volcanic activities [*Renard et al.*, 1985; *Auzende et al.*, 1996; *Embley et al.*, 1998]. There are numerous seamounts off-axis, especially on the west flank of the ridge axis [*Shen et al.*, 1993, 1995; *Scheirer et al.*, 1996]. Side-scan sonar images and the seamount volume distribution suggest that most seamounts are formed within 50 km of the ridge axis [*Shen et al.*, 1993, 1995], although some seamounts far off-axis appear to have recent magma eruptions [*Scheirer et al.*, 1996].

[6] The MELT OBSs formed two linear arrays oriented at an azimuth of about N78°E (Figure 1). The southern array crossed the ridge axis at 17°15′S, near the middle of a ridge segment with a long, continuous AMC [*Detrick et al.*, 1993]. The northern array crossed the ridge axis at 15°50′S, very close to the OSC at 15°55′S. No AMC was found for tens of kilometers on either side of this OSC [*Detrick et al.*, 1993].

[7] Each OBS was equipped with a pressure sensor (hydrophone or differential pressure gauge, DPG) and a three-component seismometer. Recording of all four channels of the 29 instruments used in this study (Table 1) was continuous at 16 samples per second. Technical problems prevented the use of other instruments in this study. The locations of the OBSs on the seafloor were determined by acoustic ranging [*Creager and Dorman*, 1982] coupled with Global Positioning System (GPS) locations of the ship [*Orcutt et al.*, 1995]. More information about instrument deployment and recovery can be found in the cruise reports by *Orcutt et al.* [1995] and *Dorman and Chave* [1996]. Unless otherwise mentioned, seismic data recorded by the Global Seismographic Network (GSN) station RPN (29.1267°S, 109.3344°W) were included in the following analyses in order to extend of the aperture of the seismic array to the south (Figure 1).

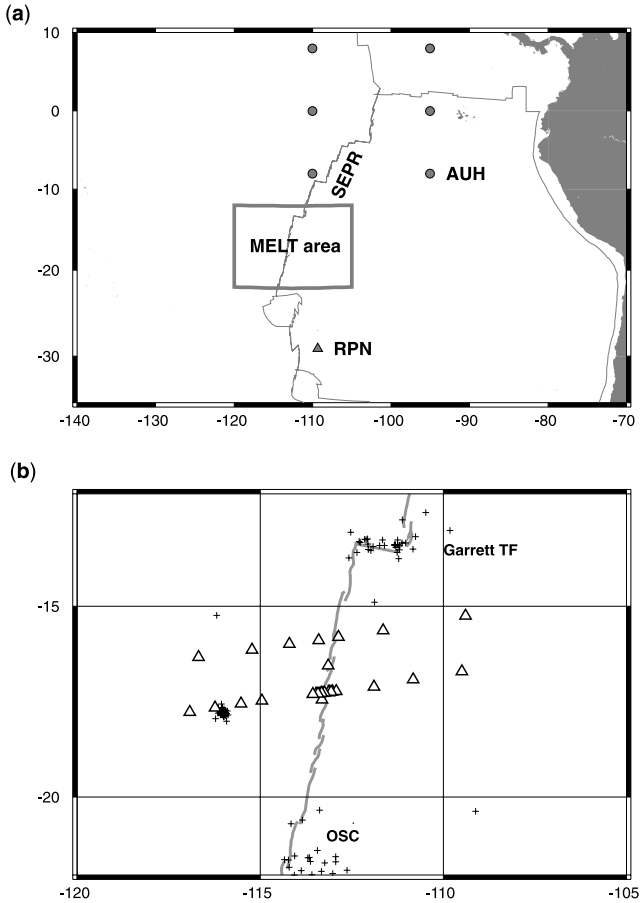

Figure 1. (a) General location of the MELT experiment at the southern East Pacific Rise. The Global Seismographic Network station RPN is shown as triangle. Dots represent the autonomous underwater hydrophones in the eastern equatorial Pacific deployed since the end of the MELT experiment. (b) Locations of the MELT ocean bottom seismometers (triangles) and the earthquakes between 1973 and 2000 listed by the National Earthquake Information Center (crosses).

3. Data Analysis

3.1. Event Detection

[8] Because of the large spacing of seismic stations and the efficiency of sound propagation in the oceanic low

Table 1. MELT OBSs and the GSN Station Used in This Study

Station	Latitude, °S	Longitude, °W	Depth, m
S01	15.2596	109.3903	3675
S03	15.6396	111.6434	3265
S05	15.8221	112.8669	2962
S07	15.9078	113.4040	3039
S08	16.0057	114.2004	3141
S09	16.1569	115.2274	3322
S10	16.3445	116.6816	3492
S11	16.5737	113.1425	3121
S13	17.2729	113.1369	3000
S14	17.2709	113.1146	2780
S15	17.2625	113.0661	2943
S16	17.2577	113.0256	3006
S18	17.2417	112.9256	3054
S26	17.1259	111.8902	3154
S28	16.9407	110.8268	3523
S30	16.7220	109.4937	3653
S32	17.2813	113.2475	3053
S33	17.2911	113.2828	3077
S34	17.2978	113.3275	3018
S35	17.3036	113.3640	3050
S36	17.3082	113.4224	3033
S37	17.3132	113.4770	3088
S38	17.3265	113.5626	3138
S45	17.4917	114.9570	3275
S46	17.5678	115.5278	3354
S47	17.6769	116.2351	3235
S48	17.7872	116.9266	3283
S50	17.4665	113.3167	3080
RPN	27.1267	109.3344	−110

sound velocity channel, T phases (the Tertiary phase) were the most frequently identified earthquake signals in OBS records. In order to process the large amount of data consistently, I developed an automated, pattern-recognition method adapted from the algorithm of *Joswig* [1990] to detect earthquake-generated T phases. Scalegrams calculated from continuous seismic records by wavelet transformation [*Kumar and Foufoula-Georgiou*, 1997] were cross-correlated with those of visually identified T phase events, air gun shots, and instrument noise, which show distinctly different patterns in the time-frequency domain (Figure 2). T phases, air gun shots, or instrument noise bursts were identified when the corresponding cross-correlation coefficients were greater than some critical values determined by visual inspection of seismic records collected in the first 2 months. Events identified with air gun shots and instrument noise bursts were not analyzed further in this study. Compared to the standard STA/LTA (Short Term Average to Long Term Average) detectors [*Allen*, 1982], the positive identification of noise patterns (air gun shots and instrumental noise bursts) gives a better detection probability without an increased false alarm rate [*Joswig*, 1990].

[9] During the 178-day experiment, 914 earthquakes generated T phases that were detected (Figure 3). On average, three T phase events per day were large enough to be recorded by at least five OBSs and their source locations were determined. The OBS array also recorded body waves from local and regional earthquakes, many of which were not listed in teleseismic earthquake catalogues. Figure 4 shows one example of the body and T waves from regional earthquakes. Body waves were usually recorded on only a few OBSs, however, and the number of earthquakes with body wave records is a small fraction of the total number of earthquakes.

3.2. T Phase Arrival Times

[10] T phases often have emergent onsets that are difficult to pick accurately. Recent T phase studies have assumed that the maximum amplitude of a T phase corresponds to the region of the seafloor with the largest conversion of seismic energy into the water column [*Slack et al.*, 1999]. Consequently, the arrival of the peak amplitude of the T phase [*Slack et al.*, 1999; *Fox et al.*, 2001] rather than the onset [e.g., *Wilcock et al.*, 1992] has been used as the arrival time of the T phase event. Because of usually broad envelopes of T phase waveforms and scattering along source-receiver paths, picking the appropriate arrival of peak amplitude remains a challenging problem. The arrival time errors and, equally importantly, the lack of objective and quantitative estimates of uncertainties in individual arrival times degrade the resolution and accuracy of T phase source locations.

[11] For any given event the envelopes of T phase waveforms at the MELT OBS array were often remarkably similar (Figure 4). I thus assessed whether the multichannel, cross-correlation method of *VanDecar and Crosson* [1990] could be adapted to estimate T phase relative travel times. Because of the complexity of T phase waveforms, I did not attempt to correlate T phases within their dominant periods (<0.5 s). I first conditioned T phase records for cross correlation by smoothening band-pass-filtered (2–6 Hz) and squared time series with a 2-s average running window. The processed data (envelopes of T wave energy) from different seismic stations were then cross-correlated to estimate relative T phase arrival times. A major advantage of the cross-correlation approach is that the uncertainty in the relative arrival time at each station can be quantitatively estimated in the least squares sense [*VanDecar and Crosson*, 1990]. The arrival time errors for T phases with good signal-to-noise ratios and coherent waveforms across the array are less than 1 s. Stations with waveforms significantly different from those at the majority of other stations, presumably due to local scattering, tend to have larger arrival time uncertainties than other stations. Since stations with larger travel time uncertainties have less weight in the inversion for T phase source locations, travel time uncertainties calculated from the cross-correlation and least squares method reflect and alleviate the problem of local scattering.

[12] For T phase events located near the OBS array (latitude 10°–25°S, longitude 105°–120°W), the average uncertainty in T phase arrival times estimated using the cross-correlation and least squares method is 2.2 s, a value comparable to the standard deviation of posterior residual times (2.6 s) but much smaller than that using the arrival time of T phase maximum amplitude (4.0 s). I conclude that for arrays with sufficiently close element spacing and coherent signals the cross-correlation and least squares method takes advantage of the array and yields statistically more robust estimates of T phase arrival times than picking T phase maximum amplitude.

3.3. T Phase Velocity

[13] T phases generated by teleseismically located, regional earthquakes (Table 2) were used to determine the

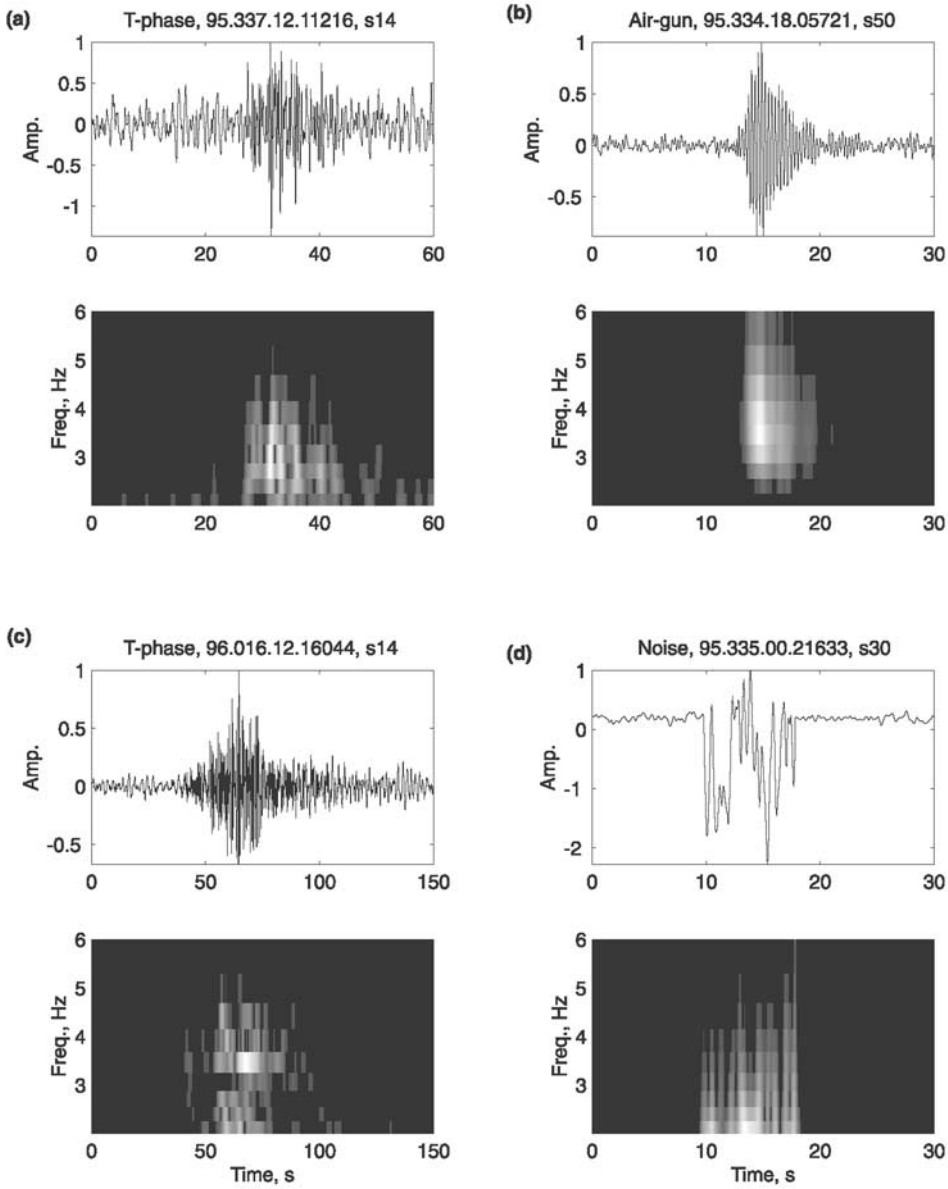

Figure 2. Waveforms and scalegrams of (a and c) two T phase events, (b) an air gun shot, and (d) an instrument noise burst.

velocity of T phase propagation. Because all regional earthquakes occurred outside the OBS array (the GSN station RPN was not used in determining the T phase velocity), the differential distances between OBSs are not sensitive to errors in epicentral locations. A least squares fit between the differential arrival times and distances yields a T phase velocity of 1476 ± 2 m/s (Figure 5), a value comparable to that in the northeast Pacific (1475 m/s) [*Slack et al.*, 1999; *Dziak*, 2001] and slightly less than the average across most of the Pacific Ocean (1484 m/s) [*Talandier and Okal*, 1998]. Evaluation of the uncertainties in T phase source locations provided later demonstrates that the T phase velocity is adequate for source-location determinations.

3.4. T Phase Source Locations and Errors

[14] I used a nonlinear, grid-search method based on work by *Rowlett and Forsyth* [1984], *Wilcock and Toomey*

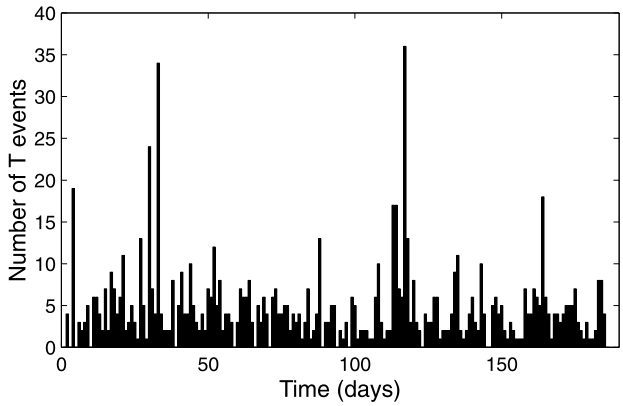

Figure 3. Number of earthquake-generated T phase events as a function of time in days since 1 November 1995.

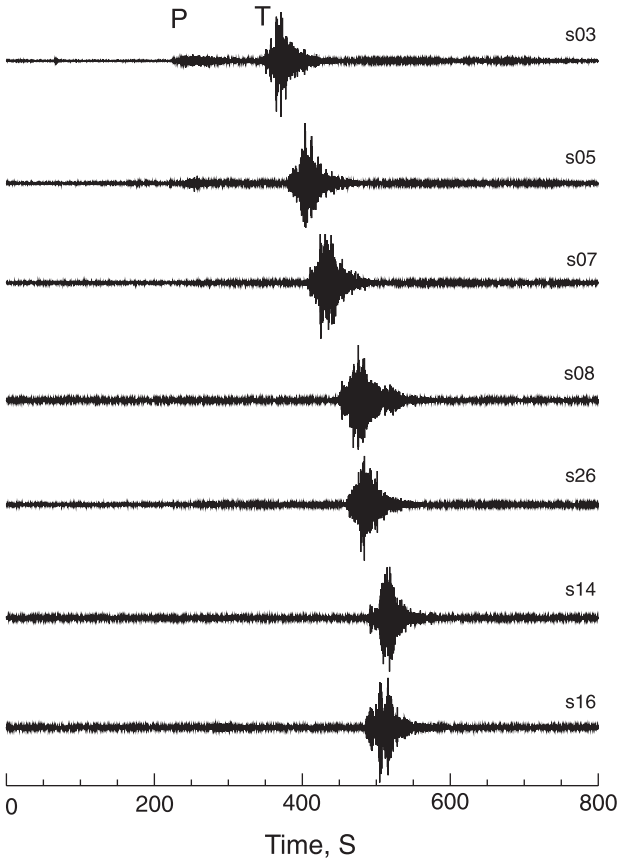

Figure 4. An example of regional earthquakes, as recorded on the vertical channel of several ocean bottom seismometers. *P* and *T* waves are identified.

[1991], and *Shen et al.* [1997] to locate T phase sources. The basis of the method is to calculate, for each event, the weighted root-mean-square (RMS) travel time residual at regularly spaced, two-dimensional grid points. An efficient, multilevel, grid-search scheme was employed to perform the search on a fine (138-m spacing) grid. For T phase events with clearly recorded body waves, both body wave and T phase relative arrival times were used to find joint solutions. The weighted root-mean-square of the travel time residual $R(\mathbf{x})$ for a source at a grid point $\mathbf{x}$ is given by

$$R(\mathbf{x}) = \mathrm{sqrt}\left[\sum_{i=2}^{n} \frac{(O_i - C_i)^2}{(n-1)\sigma_i^2}\right], \qquad (1)$$

where n is the number of arrivals, O_i is the ith travel time relative to the arrival at the reference station ($i = 1$), C_i is the relative travel time calculated for the paths from $\mathbf{x}$ to the corresponding stations, and σ_i is the travel time uncertainty for the ith station.

[15] A one-dimensional *P* and *S* wave velocity model determined from a compilation of seismic velocity structures of the normal, 1–6 Ma, oceanic crust [*Shen et al.*, 1997] was use to calculate body wave travel times. The velocity model is consistent with the one-dimensional *P* wave velocity structure beneath the MELT OBSs [*Canales et al.*, 1998], which shows small variations in the crustal thickness in the region. Because the sparse OBS array had poor constraints on the depth of local earthquakes, I assumed that the depth of the earthquake hypocenter was 3 km. Since the error in the hypocentral depth translates to a common shift in arrival times at receivers far from the epicenter, relative travel times absorb the error associated with a fixed hypocentral depth. Fixing the hypocenter at other depths had no significant effect on earthquake epicenters. A table of the minimum travel time for the first *P* and *S* arrivals was constructed from the one-dimensional velocity model using the method of *Frohlich* [1993] for a grid of horizontal distance with intervals of 110 m. The table provided body wave travel times from every two-dimensional (latitude and longitude) grid point to the stations.

[16] Two hundred and seven T phase events were located within the area shown in Figure 6. Events located outside this area tend to have larger location errors than those within this area and are not discussed hereinafter.

[17] Because most T phase events occurred outside the OBS array, the standard inversion techniques for such an event-station geometry may give a misleading evaluation of the quality of source locations [*Lilwall et al.*, 1981]. Given the availability of quantitative estimates of relative travel time uncertainties, I used a Monte Carlo approach to estimate the uncertainties in event source locations. Assuming that the uncertainties in T phase arrival times estimated from waveform cross correlation follow Gaussian distributions, I perturbed T phase arrival times randomly by an amount depending on the estimated standard deviations of arrival times at individual stations. The perturbed arrival times were used to relocate the events. This process was repeated 200 times, resulting in 200 location estimates for each event, which were then used to calculate the errors in event locations (Figure 6). This approach is different from that of *Slack et al.* [1999], in

Table 2. Teleseismically Located, Regional Earthquakes During the MELT Experiment

Event	Year	Day of Year	Time, UT	Latitude, °S	Longitude, °W	Magnitude m_b
1	1995	337	1236:33.0	23.3666	115.0887	3.8
2	1995	337	1511:55.6	23.1203	114.7307	4.7
3	1995	337	1556:23.7	24.2968	115.4584	4.1
4	1995	359	0923:32.3	8.9866	109.8939	4.2
5	1995	364	0326:11.2	4.3462	104.6227	5.2
6	1995	364	0439:05.5	4.5347	105.2404	3.6
7	1996	010	2236:46.4	5.6435	100.0753	4.3
8	1996	016	2056:34.2	24.4082	115.8612	4
9	1996	027	0505:05.8	10.3836	111.9089	3.9
10	1996	039	1712:18.9	22.6009	114.4977	3.9
11	1996	055	1123:20.5	8.6545	108.1449	4.1
12	1996	087	0407:24.1	8.7066	108.7584	4.2
13	1996	087	0408:50.0	8.7739	109.3823	4
14	1996	088	0952:35.0	24.3056	115.497	3.6
15	1996	091	0016:47.1	4.1777	102.5834	4.1
16	1996	099	1313:45.2	22.6774	114.5691	3.6
17	1996	103	1633:31.1	13.8888	113.4208	3.5
18	1996	103	2030:39.6	13.6384	112.3811	3.6
19	1996	104	0455:03.0	22.4787	113.1176	4.4
20	1996	121	0116:03.0	22.32	112.51	4.1
21	1996	122	0500:29.7	23.9602	115.41	4
22	1996	122	1848:41.4	22.62	112.207	3.9
23	1996	123	1638:46.1	22.8589	112.3151	4.2

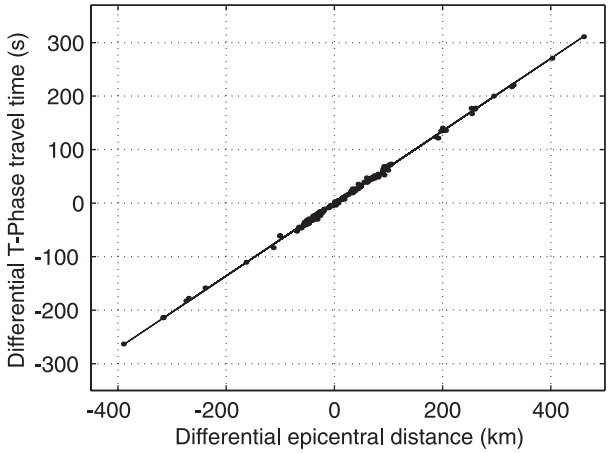

Figure 5. The least squares fit between differential T phase travel times and epicentral distances yields the T phase velocity.

which a 2-s standard deviation was used for all events at all stations.

[18] In spite of large uncertainties in T phase arrival times (2.2 s a priori and 2.6 s posterior) and the generally poor event-station geometry, the median errors (standard deviations) of the T phase source locations in the longitudinal and latitudinal directions are 3 and 6 km, respectively. Between 15°S and 18°S, where geological inferences are discussed later, the median errors in the longitudinal and latitudinal directions are 3 and 4 km, respectively. These values are much smaller than the errors in routine teleseismic locations in this region (~15 km or more) [*Hung and Forsyth*, 1996] and are comparable to the T phase location errors estimated by *Fox et al.* [2001] for the equatorial Pacific hydrophones. T phase location estimates are aided by the low sound velocity in water (1476 ± 2 m/s) and relative uniformity of the T phase velocity compared to seismic velocities in the solid Earth.

[19] The distribution of travel time residuals versus distance range is a measure of whether or not the T phase velocity used in locating the events is adequate. If the estimated velocity is significantly different from the true value, it predicts systematic variations in residual times as a function of distance. The travel time residuals show no systematic deviation from zero with distance range (Figure 7), indicating that the estimated T phase velocity is adequate for locating the events.

[20] The locations of regional earthquakes determined by land-based networks (Table 2) are systematically offset to the southwest of the corresponding T phase determinations (Figure 8). The offsets may result from errors in both teleseismic and T phase locations. An earthquake located west of the ridge axis by land-based seismic networks (event 17 in Table 2) was determined to be at the Garrett Transform Fault (13.50°S, 112.07°W) in a joint T phase and body wave determination. For this earthquake, the large location offset results primarily from errors in the teleseismic location. The source of location offsets for other earthquakes that have large location offsets but farther from the OBS array is less certain. I note that a T phase source location is not necessarily coincident with the earthquake epicenter as the seismic-acoustic conversion depends on scattering on the seafloor or in the crust [*de Groot-Hedlin and Orcutt*, 1999; *Park et al.*, 2001]. Scattering along the source-receiver path may also affect T phase locations.

[21] Almost all T phase sources at the Garrett Transform were distributed outside the fault zone represented by a deep depression in bathymetry (Figure 9). This pattern of seismicity is different from the microseismicity at the transform faults of slow spreading ridges, which is usually concentrated along the bathymetric depression [e.g., *Trehu and Solomon*, 1983; *Wilcock et al.*, 1990]. The T phase source locations at the Garrett Transform may indicate that body waves from earthquakes beneath the bathymetric depression are converted to T waves at the areas of the seafloor with high topographic features. Alternatively, acoustic energy generated in the bathymetric depression is retained inside the depression while that at high topographic features propagates outwards. The limited body waves recorded by the MELT OBSs did not provide accurate

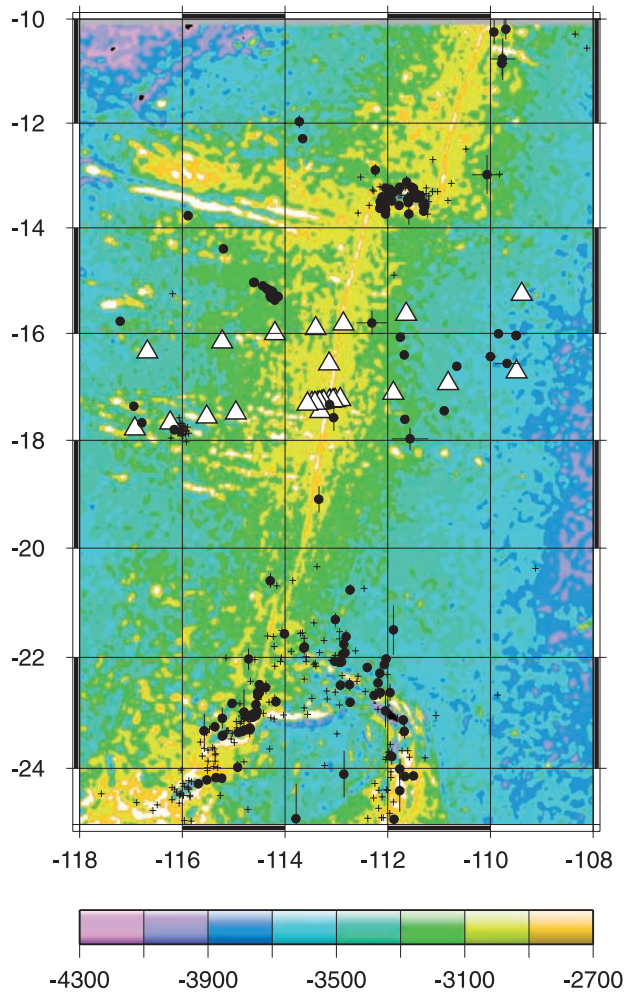

Figure 6. Distribution of the T phase events recorded during the MELT experiment (dots). Triangles represent the MELT ocean bottom seismometers. Crosses mark the locations of the earthquakes between 1973 and 2000 listed by the National Earthquake Information Center. Bathymetry is in meters.

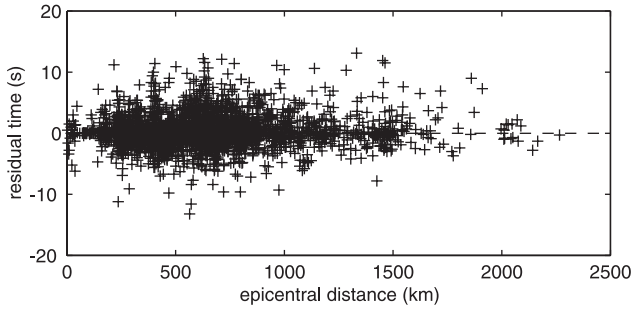

Figure 7. T phase travel time residuals as a function of distance range.

enough, independent location estimates to distinguish the two possibilities.

3.5. Magnitudes

[22] Recent T phase modeling studies have made significant progress toward understanding the mechanism by which seismic waves from earthquakes are converted to acoustic waves propagating horizontally in the water column [*de Groot-Hedlin and Orcutt*, 1999; *Park et al.*, 2001]. The results of these studies support the hypothesis that T waves arise from seismic waves scattered by a rough seafloor [e.g., *Walker et al.*, 1992; *Hildebrand et al.*, 1996] or, more generally, by lateral heterogeneity of the seafloor and crust. Further studies of T wave generation and the knowledge of seafloor topography and crustal heterogeneity near earthquake sources are required, however, before we can quantitatively assess the effects of wave conversion and propagation on the estimates of earthquake magnitudes. This lack of quantitative understanding of T phase generation has been reflected in the lack of a commonly accepted method to infer earthquake magnitudes from T phase observations. Earthquake magnitudes have been calculated from T phase acoustic amplitude [*Johnson and Northrop*, 1966; *Smith*, 1987], duration [*Okal and Talandier*, 1986], and acoustic spectral amplitude [*Hiyoshi et al.*, 1992; *Dziak et al.*, 1997; *Dziak*, 2001].

[23] Because of poor quantitative understanding of T phase generation, I opted for finding an empirical relationship between earthquake magnitudes and T phase waveforms using teleseismically located earthquakes in the region. I established a T phase magnitude scale M_T of the form

$$M_T = \sum_j \log_{10}\left(E_{ij}\right) + a\log_{10}\left(\Delta_i\right) + S_i, \qquad (2)$$

where E_{ij} is the absolute value of the T wave coda at time j on the vertical component seismometer, Δ_i is the epicentral distance from the event to the receiver, and S_i is a station correction at the ith station. I used the sum of the coda, E_i, rather than the peak-to-peak amplitude as in conventional earthquake magnitude studies because E_i is expected to be less sensitive to the dimension of the seafloor that converts seismic energy into T waves than the peak-to-peak amplitude. The dimension of the area of seafloor vibration and thus the duration of T waves increases with increasing event depth [*Schreiner et al.*, 1995; *Hildebrand et al.*, 1996; *Slack et al.*, 1999], compensating the decrease in the intensity of seafloor vibration with increasing event depth. E_i is also expected to be less affected by scattering along the source-receiver paths than the peak-to-peak amplitude. I defined T phase magnitudes equivalent to earthquake body wave magnitudes to facilitate the comparison of the two scales. Because of the limited number of regional earthquakes, I did not distinguish the styles of faults or the roughness of the seafloor near the epicenters, which may affect T phase excitation [*de Groot-Hedlin and Orcutt*, 1999; *Park et al.*, 2001; *Dziak*, 2001]. I solved simultaneously for a, S_i, and the magnitudes of regional events that minimized the misfit between teleseismic (m_b) and T phase (M_T) magnitudes in the least squares sense (Figure 10a). Care was taken to ensure that the T phase records associated with these earthquakes were not clipped. The best value for a is 2.5 ± 0.6. The scatters in m_b and M_T correlation indicate that the difference between M_T and m_b in the magnitude 3.5–5 range has a standard deviation of ~0.3.

[24] I calculated the magnitudes (M_T) of all T phases located within 2000 km of the OBS array using equation (2). A plot of T phase magnitudes versus epicentral distances (from the source to the center of the southern array) shows that the detection threshold at epicentral distances of 5°–15° is M_T = 2.0–3.5 (Figure 10b). This compares to the detection limits of m_b = 1.8–2.4 for the SOSUS array in the northeast Pacific [*Fox et al.*, 1993], m_b = 1.8 for the eastern equatorial Pacific hydrophones [*Fox et al.*, 2001], and M_w = 3.0 for the North Atlantic hydrophone array [*Smith et al.*, 2002]. These differences are due to the beam-forming capabilities of the SOSUS arrays, which provide signal gain, and the depth of the autonomous hydrophones, which are moored at the axis of the oceanic sound channel. The higher threshold for the Atlantic hydrophones is due in large part to the high level of ambient noise in the Atlantic, which masks low-magni-

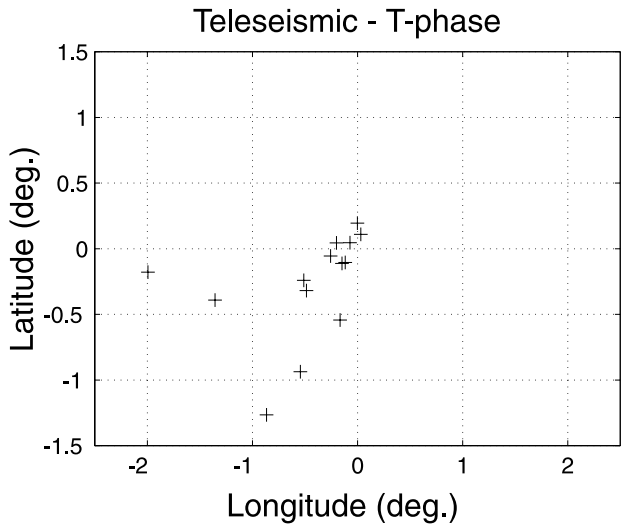

Figure 8. Differences in the locations of the regional earthquakes determined by land-based seismic networks (Table 2) and the MELT ocean bottom seismometer array.

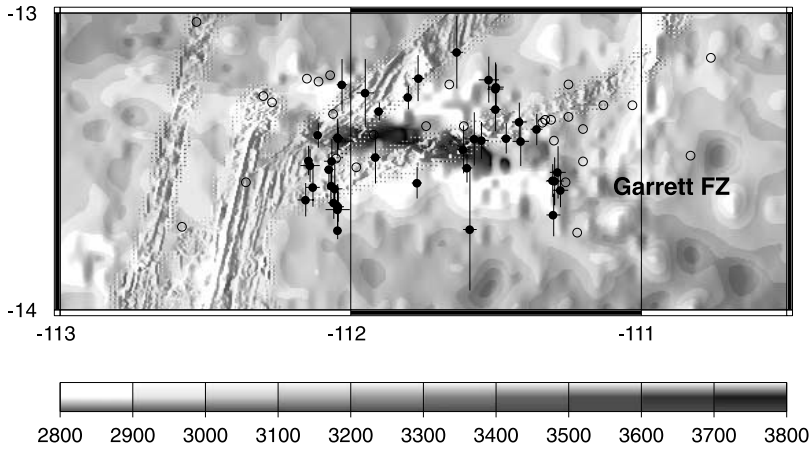

Figure 9. Locations of the T phase events near the Garrett Transform (dark dots) during the MELT experiment and the teleseismic earthquakes between 1973 and 2000 (circles). Bathymetry is in meters.

tude seismic events (C. Fox, personal communication, 2002).

4. Seismicity and Its Relationship to Tectonic and Volcanic Activities

4.1. West Flank of the SEPR

[25] Between February 1991 and May 1992, 33 earthquakes were located approximately 300 km west of the SEPR at about 18°S and 116°W by land-based seismic networks [*Hung and Forsyth*, 1996]. In December 1992, four OBSs were deployed near the teleseismic earthquake epicenters for 16 days and recorded hundreds of microearthquakes in a band about 30 km long and 6 km wide between and parallel to seamount chains (Figure 11) [*Shen et al.*, 1997]. This seismicity was interpreted as the response of the lithosphere to injection of magma from the deeper mantle primarily on the basis of variations in focal mechanisms [*Shen et al.*, 1997]. A T phase event in the area was large enough to be recorded on multiple OBSs during the MELT experiment, and was located at the western end of the 1992 microseismicity band (Figure 11).

[26] The autonomous underwater hydrophones (AUH) in the eastern equatorial Pacific have detected sporadic T phase events in the same general area since the MELT experiment (Figure 11) [*Fox et al.*, 2001]. The northeast trend of the epicenters toward the eastern equatorial Pacific hydrophones reflects typical location errors for events far outside the hydrophone array. Acoustic scattering by seamounts adjacent to the earthquake swarm may contribute to the scatter. Although the locations of the events determined from hydrophone records are not accurate enough to be confident in identifying the relationship of the events to the 1992 swarm or individual volcanic features, the close proximity suggests that they are likely associated with the T phase event during the MELT experiment and the 1992 swarm. The process that generated the 1992 seismic swarm was either reactivated during the MELT experiment or has been continuously active throughout the decade [*Fox et al.*, 2001]. This long-term activity suggests renewable stresses, which are consistent with the interpretation that magma injection was the cause of the 1992 swarm [*Shen et al.*, 1997] and inconsistent with nonrenewable, thermoelastic stresses caused by cooling of the lithosphere.

[27] A swarm of 23 earthquakes that lasted for about 2 months (from November 1995 to January 1996) was located on the west flank of the SEPR near 15.3°S, 114.5°W (Figure 6). The time-magnitude sequence of these earthquakes did not follow a typical main shock-aftershock sequence (Figure 12). Like the 1992 earthquake swarm to

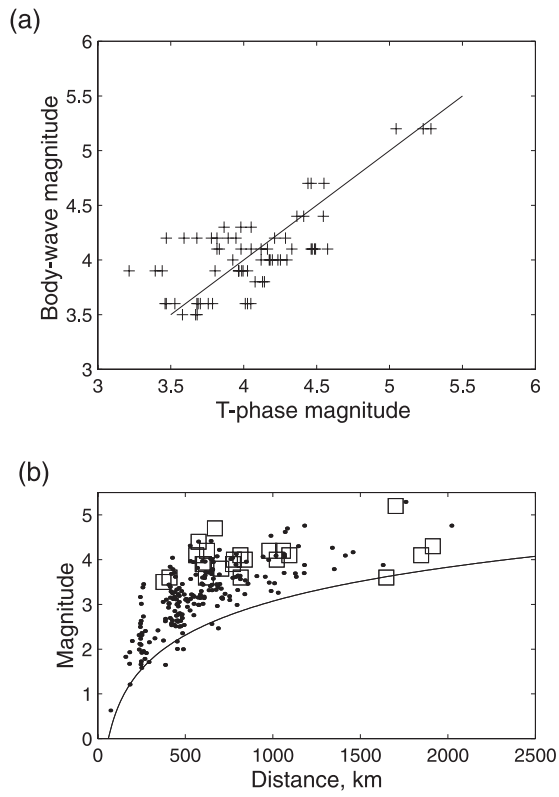

Figure 10. (a) Body wave and T phase magnitudes of the regional earthquakes during the MELT experiment. Three stations near the center of the southern array (s14, s16, and s50) are used. The line has a slope of 1. (b) Estimated magnitude of T phase events (dots) versus epicentral distance. Squares represent the body wave magnitudes of the regional earthquakes located by land-based seismic networks.

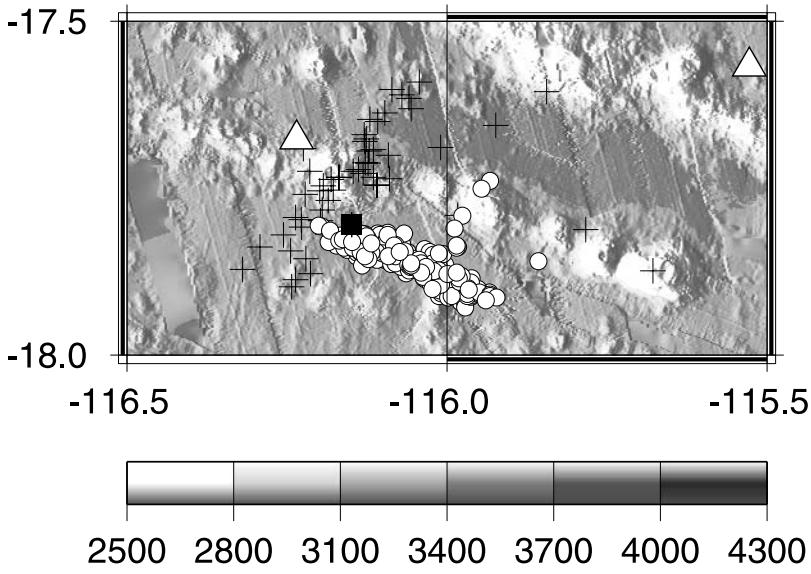

Figure 11. Locations of the T phase event (square) near the 1992 microearthquake swarm (circles). T phase events located by the eastern equatorial hydrophones since the MELT experiment are shown as crosses. Triangles represent the MELT ocean bottom seismometers. Bathymetry is in meters.

the south, the time-space sequence of this swarm did not show any obvious propagation direction. Unlike the earthquake swarm to the south, the activity stopped completely about 2 months after the first located event on 13 November 1995. The eastern equatorial Pacific hydrophones, which are capable of detecting earthquakes of the sizes in this swarm (M_T = 1.8–3.5), have not detect any earthquakes in the immediate vicinity of this swarm. Unfortunately, the site of this earthquake swarm has not been surveyed by a shipboard mapping system. It is unclear if this swarm was associated with any volcanic feature, although active volcanism in the region can be inferred from the geoid-derived bathymetry and shipboard surveys in adjacent areas.

4.2. East Flank of the SEPR

[28] In sharp contrast to the swarm characteristics of earthquakes on the west flank of the ridge axis, earthquakes on the Nazca flank appeared to be randomly distributed in time and space (Figure 6). They did not appear to be associated with seamount chains and thus represented the background seismicity, which was nearly absent on the Pacific flank. The difference in the apparent background seismicity between the east and west flanks of the ridge axis could result from an insufficient recording period, or more likely the difference in the thermal structure of the Pacific and Nazca plates. From the Wilkes Transform (9°S) to the Easter Microplate (23°S), the Nazca flank subsides at about twice the rate of the Pacific flank [*Cochran*, 1986; *Scheirer et al.*, 1998], indicating that, at a given distance from the ridge axis, the Nazca plate is thicker and stronger than the Pacific plate. Faster cooling (thus greater variations in thermoelastic stresses) and a stronger lithosphere were two possible factors that aided the generation of moderate earthquakes on the Nazca plate recorded by multiple OBSs.

4.3. Ridge Axis

[29] Only two T phase events were located at the ridge axis near the southern array, where the station spacing was relatively small (Figure 6). The larger event had an estimated magnitude (M_T) of 0.5, a value much smaller than the detection threshold of land-based seismic networks and that of the eastern equatorial Pacific hydrophones ($m_b \sim 1.8$). The small earthquake magnitudes are consistent with the presence of shallow magma chambers and, by inference, a thin elastic layer at the ridge axis.

[30] The low seismicity rate along the ridge axis was the consequence of the low magnitudes of earthquakes at the ridge axis and the inadequacy of the MELT OBS array to locate these very small earthquakes. A comparison of repeated bathymetric surveys of the ridge axis between 16°S and 18°40′S in late 1995, late 1996, and mid-1997 detected no significant seafloor topographic changes, indicating that no significant magma eruption occurred during that period [*Dunn et al.*, 2001]. The low seismicity rate at the ridge axis should not be interpreted as evidence for the lack of dike intrusions at the ridge axis, however. Earthquakes associated with diking at the SEPR are likely to be

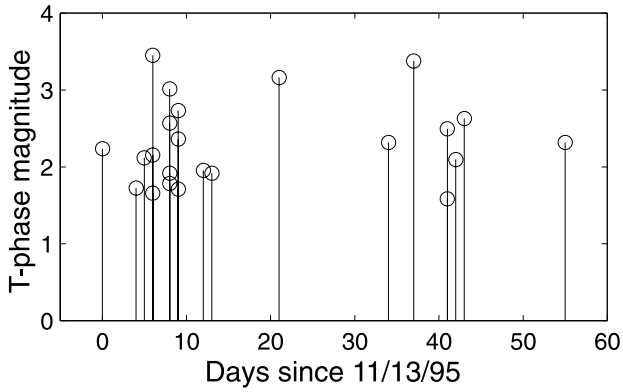

Figure 12. T phase magnitudes of the earthquake swarm near 15.3°S, 114.5°W versus time in days since 13 November 1995.

much smaller than those associated with diking events at the Juan de Fuca Ridge [*Fox et al.*, 1995; *Dziak et al.*, 1995; *Schreiner et al.*, 1995] and the detection thresholds of the MELT OBS array. For the same reason, earthquakes generated by faulting within a few tens of kilometers of this fast spreading center might also be too small to be located.

5. Conclusions

[31] This study demonstrates that ocean bottom seismometers can be used to detect and locate T phase events. Over 200 T phase events were located near the MELT OBS array. Using an empirical relationship between earthquake magnitudes and T wave waveforms, I estimated that the T phase detection thresholds of the OBS array were magnitudes (M_T) 2–3.5 at epicentral distances of 5°–15°. The MELT OBSs and subsequent equatorial Pacific hydrophones recorded earthquakes near an earthquake swarm in 1992, which was located approximately 300 km west of the ridge axis at about 18°S and 116°W. The earthquake process that generated the 1992 swarm was either reactivated 3 years later during the OBS experiment or has been continuously active in the past decade. This long-term activity suggests renewable stresses, which are consistent with the interpretation that magma injection was the cause of the 1992 swarm [*Shen et al.*, 1997]. A swarm of earthquakes located near 15.3°S, 114.5°W on the west flank of the SEPR lasted for about 2 months during the OBS experiment. In contrast to the swarm characteristics of earthquakes on the west flank of the ridge axis, earthquakes on the Nazca flank were randomly distributed in time and space. The difference in seismicity between the Pacific and Nazca flanks may result from the difference in the thermal structure of the Pacific and Nazca plates. The few earthquakes located at the ridge axis had very small magnitudes, reflecting the presence of shallow magma chambers beneath the ridge axis and the thin elastic layer of the fast spreading SEPR. This result also indicates that acoustic monitoring of earthquakes associated with dike intrusion is difficult at regional scales at this fast spreading ridge. There is no apparent correlation between seismicity and off-axis seamounts.

[32] **Acknowledgments.** L. Dorman and S. Webb kindly provided OBS data collected by their groups. I thank other participants in the MELT experiment for providing the opportunity of this study. Sarah McDonald helped the initial processing of the OBS data. C. Fox and the Associate Editor provided constructive reviews of the manuscript. The GMT plotting package of *Wessel and Smith* [1991] was used to prepare figures. This study was supported by the National Science Foundation under the grant OCE-9896393.

References

Allen, R., Automatic phase pickers: Their present use and future prospects, *Bull. Seismol. Soc. Am.*, *72*, S225–S242, 1982.

Azende, J.-M., et al., Recent tectonic, magmatic, and hydrothermal activity on the East Pacific Rise between 17°S and 19°S: Submersible observations, *J. Geophys. Res.*, *101*, 17,995–18,010, 1996.

Bergman, E. A., and S. C. Solomon, Source mechanisms of earthquakes near mid-ocean ridges from body waveform inversion: Implications for the early evolution of oceanic lithosphere, *J. Geophys. Res.*, *89*, 11,415–11,441, 1984.

Bratt, S. R., E. A. Bergman, and S. C. Solomon, Thermoelastic stress: How important as a cause of earthquakes in young oceanic lithosphere?, *J. Geophys. Res.*, *90*, 10,249–10,260, 1985.

Canales, J. P., R. S. Detrick, S. Bazin, A. J. Harding, and J. A. Orcutt, Off-axis crustal thickness across and along the East Pacific Rise within the MELT area, *Science*, *280*, 1218–1221, 1998.

Carbotte, S., and K. C. Macdonald, Comparison of seafloor tectonic fabric created at intermediate, fast, and superfast spreading ridges: Influence of spreading rate, plate motions, and ridge segmentation on fault patterns, *J. Geophys. Res.*, *99*, 13,609–13,631, 1994.

Chadwick, W. W., Is the "axial summit caldera" on the East Pacific Rise really a "graben", *RIDGE Events*, *8*, 8–11, 1997.

Cochran, J. R., Variations in subsidence rates along intermediate and fast-spreading, mid-ocean ridges, *Geophys. J. R. Astron. Soc.*, *87*, 421–459, 1986.

Cormier, M.-H., D. S. Scheirer, and K. C. Macdonald, Evolution of the East Pacific Rise at 16–19°S since 5 Ma: Bisection of overlapping spreading centers by new rapidly propagating ridge segments, *Mar. Geophys. Res.*, *18*, 53–84, 1996.

Creager, K. C., and L. M. Dorman, Location of instruments on the seafloor by joint adjustment of instrument and ship positions, *J. Geophys. Res.*, *87*, 8379–8388, 1982.

de Groot-Hedlin, C. D., and J. A. Orcutt, Synthesis of earthquake-generated T-waves, *Geophys. Res. Lett.*, *26*, 1227–1230, 1999.

Denlinger, R. P., and W. Z. Savage, Thermal stresses due to cooling of a viscoelastic oceanic lithosphere, *J. Geophys. Res.*, *94*, 744–752, 1989.

Detrick, R. S., A. J. Harding, G. M. Kent, J. A. Orcutt, J. C. Mutter, and P. Buhl, Seismic structure of the southern East Pacific Rise, *Science*, *259*, 499–503, 1993.

Dorman, L. M., and A. Chave, OBS recovery and EM deployment cruise report, Scripps Inst. of Oceanography, La Jolla, Calif., 1996.

Dunn, R. A., D. S. Scheirer, and D. W. Forsyth, A detailed comparison of repeated bathymetric surveys along a 300-km-long section of the southern East Pacific Rise, *J. Geophys. Res.*, *106*, 463–471, 2001.

Dziak, R. P., Empirical relationship of T-wave energy and fault parameters of northeast Pacific Ocean earthquakes, *Geophys. Res. Lett.*, *28*, 2537–2540, 2001.

Dziak, R. P., C. G. Fox, and A. E. Schreiner, The June–July 1993 seismo-acoustic event at CoAxial segment, Juan de Fuca Ridge: Evidence for a lateral dike injection, *Geophys. Res. Lett.*, *22*, 135–138, 1995.

Dziak, R. P., C. G. Fox, H. Matsumoto, and A. E. Schreiner, The April 1992 Cape Mendocino earthquake sequence: Seismo-acoustic analysis utilizing fixed hydrophone arrays, *Mar. Geophys. Res.*, *19*, 137–162, 1997.

Embley, R. W., J. E. Lupton, G. Massoth, T. Urabe, V. Tunnicliffe, D. A. Butterfield, T. Shibata, O. Okano, M. Kinoshita, and K. Fujioka, Geological, chemical, and biological evidence for recent volcanism at 17.5°S: East Pacific Rise, *Earth Planet. Sci. Lett.*, *163*, 131–147, 1998.

Fornari, D. J., T. Gregg, and M. R. Perfit, Axial summit caldera and axial summit graben: A reply, *RIDGE Events*, *8*, 12–19, 1997.

Forsyth, D. W., et al., Imaging the deep structure beneath a mid-ocean ridge: The MELT experiment, *Science*, *280*, 1215–1218, 1998.

Fox, C. G., R. P. Dziak, H. Matsumoto, and A. E. Schreiner, Potential for monitoring low-level seismicity on the Juan de Fuca Ridge using military hydrophone arrays, *Mar. Technol. Soc. J.*, *27*, 22–30, 1993.

Fox, C. G., W. E. Radford, R. P. Dziak, T.-K. Lau, H. Matsumoto, and A. E. Schreiner, Acoustic detection of a seafloor spreading episode on the Juan de Fuca Ridge using military hydrophone arrays, *Geophys. Res. Lett.*, *22*, 131–134, 1995.

Fox, C. G., H. Matsumoto, and T.-K. A. Lau, Monitoring Pacific Ocean seismicity from an autonomous hydrophone array, *J. Geophys. Res.*, *106*, 4183–4206, 2001.

Frohlich, C., Users manual for TexFlex-0.5: The Texas flexible, practical program package for locating seismic events, *Tech. Rep. 128*, 66 pp., Inst. for Geophys., Univ. of Tex., Austin, 1993.

Haxby, W. F., and J. K. Weissel, Evidence for small-scale mantle convection from Seasat altimeter data, *J. Geophys. Res.*, *91*, 3507–3520, 1986.

Haymon, R. M., D. J. Fornari, M. H. Edwards, S. M. Carbotte, D. Wright, and K. C. Macdonald, Hydrothermal vent distribution along the East Pacific Rise crest (9°09′–54′N) and its relationship to magmatic and tectonic processes on fast-spreading mid-ocean ridges, *Earth Planet. Sci. Lett.*, *104*, 513–534, 1991.

Hildebrand, J., C. G. Fox, and R. P. Dziak, A multipath model for T-wave generation by seafloor earthquakes, *J. Acoust. Soc. Am.*, *100*, 2639, 1996.

Hiyoshi, Y., D. A. Walker, and C. S. McCreery, T-phase data and regional tsunami genesis in Japan, *Bull. Seismol. Soc. Am.*, *82*, 2213–2223, 1992.

Hung, S.-H., and D. W. Forsyth, Non-double-couple focal mechanisms in an oceanic, intraplate earthquake swarm: Application of an improved method for comparative event, moment tensor determination, *J. Geophys. Res.*, *101*, 25,347–25,371, 1996.

Johnson, R. H., and J. Northrop, A comparison of earthquake magnitude with T-phase strength, *Bull. Seismol. Soc. Am.*, *56*, 119–124, 1966.

Joswig, M., Pattern recognition for earthquake detection, *Bull. Seismol. Soc. Am.*, *80*, 170–186, 1990.

Kumar, P., and E. Foufoula-Georgiou, Wavelet analysis for geophysical applications, *Rev. Geophys.*, *35*, 385–412, 1997.

Lee, S.-M., and S. C. Solomon, Constraints from SeaBeam bathymetry on the development of normal faults on the East Pacific Rise, *Geophys. Res. Lett.*, *22*, 3135–3138, 1995.

Lilwall, R. C., T. J. G. Francis, and I. T. Porter, A microearthquake survey at the junction of the East Pacific Rise and the Wilker (9°S) Fracture Zone, *Geophys. J. R. Astron. Soc.*, *66*, 407–416, 1981.

Lonsdale, P., Segmantation of the Pacific-Nazca spreading center, 1°N–20°S, *J. Geophys. Res.*, *94*, 12,197–12,225, 1989.

Macdonald, K. C., and P. J. Fox, The axial summit graben and cross-sectional shape of the East Pacific Rise as indicator of axial magma chambers and recent volcanic eruptions, *Earth. Planet. Sci. Lett.*, *88*, 119–131, 1988.

Macdonald, K. C., P. J. Fox, R. T. Alexander, R. Pockalny, and P. Gente, Volcanic growth faults and the origin of Pacific abyssal hills, *Nature*, *380*, 125–129, 1996.

Norris, R. A., and R. H. Johnson, Submarine volcanic eruptions recently located in the Pacific by SOFAR hydrophones, *J. Geophys. Res.*, *74*, 650–664, 1969.

Okal, E. A., and J. Talandier, T-wave duration, magnitudes and seismic moment of an earthquake: Application to tsunami warning, *J. Phys. Earth*, *34*, 19–42, 1986.

Okal, E. A., J. Talandier, K. A. Sverdrup, and T. H. Jordan, Seismicity and tectonic stress in the south central Pacific, *J. Geophys. Res.*, *85*, 6479–6495, 1980.

Orcutt, J. A., R. S. Detrick, L. M. Dorman, D. W. Forsyth, and S. C. Webb, Mantle Electromagnetic and Tomography (MELT) cruise report, Scripps Inst. of Oceanography, La Jolla, Calif., 1995.

Park, M., R. I. Odom, and D. J. Soukup, Modal scattering: A key to understanding oceanic T-waves, *Geophys. Res. Lett.*, *17*, 3401–3404, 2001.

Renard, V., R. Hekinian, J. Francheteau, R. D. Ballard, and H. Backer, Submersible observations at the axis of the ultra-fast-spreading East Pacific Rise (17°30′ to 21°30′S), *Earth Planet. Sci. Lett.*, *75*, 339–353, 1985.

Rowlett, H., and D. W. Forsyth, Recent faulting and microearthquakes at the intersection of the Vema Fracture Zone and the Mid-Atlantic Ridge, *J. Geophys. Res.*, *89*, 6079–6094, 1984.

Sandwell, D. T., E. L. Winterer, J. Mammerickx, R. A. Duncan, M. A. Lynch, D. A. Levitt, and C. L. Johnson, Evidence for diffuse extension of the Pacific plate from Pukapuka ridges and cross-grain gravity lineations, *J. Geophys. Res.*, *100*, 15,087–15,099, 1995.

Scheirer, D. S., K. C. Macdonald, D. W. Forsyth, and Y. Shen, Abundant seamounts of the Reno Rahi seamount field near the southern East Pacific Rise, 15°S to 19°S, *Mar. Geophys. Res.*, *18*, 13–52, 1996.

Scheirer, D. S., D. W. Forsyth, M.-H. Cormier, and K. C. Macdonald, Shipboard geophysical indications of asymmetry of melt production beneath the East Pacific Rise near the MELT experiment, *Science*, *280*, 1221–1224, 1998.

Schreiner, A. E., C. G. Fox, and R. P. Dziak, Spectra and magnitudes of T-waves from the 1993 earthquake swarm on the Juan de Fuca Ridge, *Geophys. Res. Lett.*, *22*, 139–142, 1995.

Shen, Y., D. W. Forsyth, D. S. Scheirer, and K. C. Macdonald, Two forms of volcanism: Implications for mantle flow and off-axis crustal production on the west flank of the southern East Pacific Rise, *J. Geophys. Res.*, *98*, 17,875–17,889, 1993.

Shen, Y., D. S. Scheirer, D. W. Forsyth, and K. C. Macdonald, Trade-off in production between adjacent seamount chains near the southern East Pacific Rise (17–19°S), *Nature*, *373*, 140–143, 1995.

Shen, Y., D. W. Forsyth, J. Conder, and L. M. Dorman, Investigation of microearthquake activity following an intraplate teleseismic swarm on the west flank of the southern East Pacific Rise, *J. Geophys. Res.*, *102*, 459–475, 1997.

Sinton, J. M., S. M. Smaglik, J. J. Mahoney, and K. C. Macdonald, Magmatic processes at superfast mid-ocean ridges: Glass compositional variations along the East Pacific Rise 13–23°S, *J. Geophys. Res.*, *96*, 6133–6155, 1991.

Slack, P. D., C. G. Fox, and R. P. Dziak, *P* wave detection thresholds, *Pn* velocity estimates, and *T* wave location uncertainty from oceanic hydrophones, *J. Geophys. Res.*, *104*, 13,061–13,073, 1999.

Smith, D. K., M. Tolstoy, C. G. Fox, D. R. Bohnenstiehl, H. Matsumoto, and M. J. Fowler, Hydroacoustic monitoring of seismicity at the slow-spreading Mid-Atlantic Ridge, *Geophys. Res. Lett.*, *29*(11), 1518, doi:10.1029/2001GL013912, 2002.

Smith, W. D., Underground nuclear explosions recorded at Rarotonga: Estimation of m_b from T-phase amplitude, *Geophys. J. R. Astron. Soc.*, *90*, 35–42, 1987.

Talandier, J., and E. A. Okal, On the mechanism of conversion of seismic waves to and from *T* waves in the vicinity of island shores, *Bull. Seismol. Soc. Am.*, *88*, 621–632, 1998.

Trehu, A. M., and S. C. Solomon, Earthquakes in the Orozco Transform Zone: Seismicity, source mechanisms, and tectonics, *J. Geophys. Res.*, *88*, 8203–8225, 1983.

VanDecar, J. C., and R. S. Crosson, Determination of teleseismic relative phase arrival times using multi-channel cross-correlation and least squares, *Bull. Seismol. Soc. Am.*, *80*, 150–159, 1990.

Walker, D. A., C. S. McCreery, and Y. Hiyoshi, T-phase spectra, seismic moments, and tsunamigenesis, *Bull. Seismol. Soc. Am.*, *82*, 1275–1305, 1992.

Wessel, P., and W. H. F. Smith, Free software helps map and display data, *Eos Trans. AGU*, *72*(441), 445–446, 1991.

Wiens, D. A., and S. Stein, Age dependence of oceanic intraplate seismicity and implications for lithospheric evolution, *J. Geophys. Res.*, *88*, 6455–6458, 1983.

Wiens, D. A., and S. Stein, Intraplate seismicity and stresses in young oceanic lithosphere, *J. Geophys. Res.*, *89*, 11,442–11,464, 1984.

Wilcock, W. S. D., and D. R. Toomey, Estimating hypocentral uncertainties for microearthquake surveys conducted at sea: A comparison of generalized inversion and grid search methods, *Mar. Geophys. Res.*, *13*, 161–171, 1991.

Wilcock, W. S. D., G. M. Purdy, and S. C. Solomon, Microearthquake evidence for extension across the Kane transform fault, *J. Geophys. Res.*, *95*, 15,439–15,462, 1990.

Wilcock, W. S. D., G. M. Purdy, S. C. Solomon, D. L. DuBois, and D. R. Toomey, Microearthquakes on and near the East Pacific Rise, 9–10°N, *Geophys. Res. Lett.*, *19*, 2131–2134, 1992.

Wysession, M. E., E. A. Okal, and K. L. Miller, Intraplate seismicity of the Pacific Basin, 1913–1988, *Pure Appl. Geophys.*, *135*, 261–359, 1991.

Wysession, M. E., J. Wilson, L. Bartko, and R. Sakata, Intraplate seismicity in the Atlantic Ocean Basin: A teleseismic catalog, *Bull. Seismol. Soc. Am.*, *85*, 755–774, 1995.

Y. Shen, University of Rhode Island, Graduate School of Oceanography, South Ferry Road, Narragansett, RI 02882, USA. (yang@island.gso.uri.edu)